AGU PUBLICATIONS

Paleoceanography

RESEARCH ARTICLE
10.1002/2016PA003020

Key Points:
- Benthic I/Ca can be used as bottom water (epifaunal) and pore water (infaunal) redox proxies
- Benthic I/Ca with Mn oxide EF, Ce anomaly, and climate models suggest oxygenated deep Atlantic and possible widespread low O_2 intermediate water
- Higher total iodine concentration in seawater in the late Paleocene than at present

Supporting Information:
- Supporting Information S1
- Table S1

Correspondence to:
Z. Lu,
zunlilu@syr.edu

Citation:
Zhou, X., E. Thomas, A. M. E. Winguth, A. Ridgwell, H. Scher, B. A. A. Hoogakker, R. E. M. Rickaby, and Z. Lu (2016), Expanded oxygen minimum zones during the late Paleocene-early Eocene: Hints from multiproxy comparison and ocean modeling, *Paleoceanography*, *31*, 1532–1546, doi:10.1002/2016PA003020.

Received 10 AUG 2016
Accepted 2 NOV 2016
Accepted article online 11 NOV 2016
Published online 10 DEC 2016

Expanded oxygen minimum zones during the late Paleocene-early Eocene: Hints from multiproxy comparison and ocean modeling

X. Zhou[1], E. Thomas[2,3], A. M. E. Winguth[4], A. Ridgwell[5,6], H. Scher[7], B. A. A. Hoogakker[8], R. E. M. Rickaby[8], and Z. Lu[1]

[1]Department of Earth Sciences, Syracuse University, Syracuse, New York, USA, [2]Department of Geology and Geophysics, Yale University, New Haven, Connecticut, USA, [3]Department of Earth and Environmental Sciences, Wesleyan University, Middletown, Connecticut, USA, [4]Department of Earth and Environmental Sciences, University of Texas at Arlington, Arlington, Texas, USA, [5]Department of Earth Sciences, University of California, Riverside, California, USA, [6]School of Geographical Sciences, University of Bristol, Bristol, UK, [7]Department of Earth and Ocean Sciences, University of South Carolina, Columbia, South Carolina, USA, [8]Department of Earth Sciences, University of Oxford, Oxford, UK

Abstract Anthropogenic warming could well drive depletion of oceanic oxygen in the future. Important insight into the relationship between deoxygenation and warming can be gleaned from the geological record, but evidence is limited because few ocean oxygenation records are available for past greenhouse climate conditions. We use I/Ca in benthic foraminifera to reconstruct late Paleocene through early Eocene bottom and pore water redox conditions in the South Atlantic and Southern Indian Oceans and compare our results with those derived from Mn speciation and the Ce anomaly in fish teeth. We conclude that waters with lower oxygen concentrations were widespread at intermediate depths (1.5–2 km), whereas bottom waters were more oxygenated at the deepest site, in the Southeast Atlantic Ocean (>3 km). Epifaunal benthic foraminiferal I/Ca values were higher in the late Paleocene, especially at low-oxygen sites, than at well-oxygenated modern sites, indicating higher seawater total iodine concentrations in the late Paleocene than today. The proxy-based bottom water oxygenation pattern agrees with the site-to-site O_2 gradient as simulated in a comprehensive climate model (Community Climate System Model Version 3), but the simulated absolute dissolved O_2 values are low (< ~35 μmol/kg), while higher O_2 values (~60–100 μmol/kg) were obtained in an Earth system model (Grid ENabled Integrated Earth system model). Multiproxy data together with improvements in boundary conditions and model parameterization are necessary if the details of past oceanographic oxygenation are to be resolved.

1. Introduction

1.1. Ocean Deoxygenation During Periods of Global Warming

Recent ocean warming may already have contributed to a decrease in dissolved oxygen concentrations in the oceans [*Falkowski et al.*, 2011; *Helm et al.*, 2011]. Less oxygen dissolves in seawater at higher temperatures [*Weiss*, 1970], and transient surface warming leads to increased stratification and hence reduced ventilation. Oxygen minimum zones (OMZs) may have expanded and shoaled over the last 50 years, affecting valuable fisheries [*Stramma et al.*, 2008; *Reid et al.*, 2009; *Keeling et al.*, 2010]. Records covering the previous century, however, suggest that recent global warming probably was not the only factor, and decadal time scale oceanographic fluctuations may have contributed to changing ocean oxygen levels [e.g., *Falkowski et al.*, 2011; *Deutsch et al.*, 2014]. On longer time scales, warming may drive intensified continental weathering, delivering a greater nutrient flux to the ocean [e.g., *Pierrehumbert*, 2002; *Wild and Liepert*, 2010]. Other things being equal, this increased nutrient inventory will stimulate productivity, organic matter export fluxes, hence greater oxygen consumption in the ocean interior [e.g., *McInerney and Wing*, 2011; *Giusberti et al.*, 2016]. In addition, under higher oceanic temperatures, the remineralization of organic matter in the water column may have proceeded faster at higher metabolic rates in warmer waters, thus have been more efficient and occurred at shallower depths [*Olivarez Lyle and Lyle*, 2006; *Boscolo-Galazzo et al.*, 2014; *John et al.*, 2014; *Ma et al.*, 2014]. These processes will influence oceanic dissolved oxygen concentrations in different ways at different locations, and some will combine nonlinearly (e.g., stratification and remineralization with biological productivity), making it difficult to project the extent and severity of ocean deoxygenation induced by global warming. Investigating the evolution of oxygen content in the ocean interior across past global

warming events could provide analogs to anthropogenic climate change and help us understand the extent and possible mechanisms of future ocean deoxygenation.

Ocean redox changes have been studied intensively across episodes of extreme warming and oxygen depletion, such as the Oceanic Anoxic Events of the Jurassic and Cretaceous [e.g., *Jenkyns*, 2010; *Lu et al.*, 2010]. However, these events may not provide the best geological analogs for predicting ocean deoxygenation in the Anthropocene, because of the extreme conditions and very different tectonic configuration of the continents and ocean basins during these events. The greenhouse conditions during the Paleogene may be more similar to the future challenges to human society [e.g., *Norris et al.*, 2013].

Global climate in the late Paleocene-early Eocene was overall warm, and there probably were no polar ice sheets. Superimposed on this "greenhouse climate" were short periods of extreme global warming, the hyperthermal events. The Paleocene Eocene Thermal Maximum (PETM, ~56 Ma) was the most extreme of these and was an abrupt, transient period of global warming characterized by a surface ocean warming of at least 4–5°C [*Dunkley Jones et al.*, 2013], with the transition into this event possibly occurring over a few kiloyears [*Zeebe et al.*, 2014; *Kirtland Turner and Ridgwell*, 2016; *Zeebe et al.*, 2016]. It has been speculated that the early Paleogene oceans were less oxygenated compared to today [*Norris et al.*, 2013] based on the benthic foraminiferal oxygen index (BFOI) [*Kaiho*, 1994], but this speculation is qualitative, and the index has not been supported in studies of living benthic foraminifera [e.g., *Gooday*, 2003; *Jorissen et al.*, 2007]. However, several other lines of evidence suggest at least large-scale regional ocean deoxygenation during the PETM [e.g., *Dickson et al.*, 2012, 2014]. I/Ca data on planktonic foraminifera indicate expanded OMZs in the upper water column of major oceans [*Zhou et al.*, 2014], which may be related to the increase of the temperature-dependent remineralization rate, thus more intense O_2 depletion at shallow depths [e.g., *John et al.*, 2014]. Bottom water oxygen depletion occurred in marginal basins of the Tethys and peri-Tethys [e.g., *Canudo et al.*, 1995; *Speijer*, 1997; *Bolle et al.*, 2000; *Gavrilov et al.*, 2003; *Soliman et al.*, 2011; *Dickson et al.*, 2014; *Giusberti et al.*, 2016], along continental margins such as New Jersey [*Lippert and Zachos*, 2007; *Stassen et al.*, 2012, 2015] and New Zealand [*Nicolo et al.*, 2010], and in the Arctic Ocean [*Sluijs et al.*, 2006].

However, evidence for oxygenation changes in the deep open ocean is less clear. This is important because the only major extinction occurring across the PETM was among benthic foraminifera, and reduced oxygen availability is at least part of the leading explanations [e.g., *Thomas*, 1989; *Kennett and Stott*, 1991; *Kaiho et al.*, 1996; *Thomas*, 2003], though not supported at all locations [*Thomas*, 2007; *Alegret et al.*, 2010]. Redox-sensitive trace metals indicate low-oxygen bottom waters at bathyal (1000–3000 m) but not abyssal (>3000 m) depths before and after the PETM on Walvis Ridge in the South Atlantic Ocean and deoxygenation from bathyal to abyssal depths during the PETM in the same region [*Chun et al.*, 2010]. Very transient deoxygenation (during the interval of noncarbonate deposition) may have occurred even at abyssal depths, as indicated by the presence of an unusual Mn-oxide mineral, jianshuiite, possibly formed during the recovery from pore water deoxygenation [*Post et al.*, 2016]. Mn enrichment data suggest that suboxic sedimentary conditions occurred prior to, during, and in the recovery from the PETM at intermediate depth sites in the Atlantic and Southern Oceans, whereas Pacific sites remained relatively oxygenated [*Pälike et al.*, 2014].

Here we supplement trace-metal-based approaches by using the novel redox proxy of I/Ca in benthic foraminiferal tests to reconstruct bottom water and pore water oxygenation conditions in the late Paleocene through early Eocene in the South Atlantic and Southern Indian Ocean. We have very few I/Ca data during the PETM itself due to the scarcity and small size of benthic foraminiferal tests directly after the benthic foraminiferal extinction event, so we evaluate general oceanic conditions during the overall warm period of the late Paleocene-early Eocene. We also report Ce anomaly data in fish teeth to compare with the I/Ca and published Mn speciation records [*Chun et al.*, 2010; *Pälike et al.*, 2014]. We then compare all data to dissolved oxygen contents of bottom waters in the late Paleocene as simulated from Community Climate System Model Version 3 (CCSM3) [*Collins et al.*, 2006; *Winguth et al.*, 2010, 2012] and an Earth system model (Grid ENabled Integrated Earth system model (cGENIE)) [e.g., *Ridgwell et al.*, 2007].

1.2. I/Ca as a Redox Proxy

Iodate (IO_3^-) and iodide (I^-) are the stable chemical forms of iodine in seawater and comprise the total iodine concentration in the ocean. The relative abundance of iodate and iodide depends on the redox condition of

seawater, with iodate dominant in well-oxygenated waters, and iodide in anoxic waters [*Rue et al.*, 1997]. Only iodate is incorporated into the carbonate lattice, possibly due to the large ionic radius of I^- [*Lu et al.*, 2010, and the references therein]. Since iodate enters the calcite lattice in proportion to the iodate concentration in ambient seawater, I/Ca in calcite should reflect the iodate level, thus redox conditions of seawater [*Lu et al.*, 2010]. I/Ca in planktonic [*Zhou et al.*, 2014; *Lu et al.*, 2016] and benthic foraminifera [*Glock et al.*, 2014] test calcite were shown to reflect ocean redox conditions. Benthic foraminifera calcify on the ocean floor or within the sediment, and thus should record the iodate concentrations, indicating oxygenation levels in the bottom and/or pore water. Other than redox conditions, their I/Ca values may also be controlled by total iodine concentration in bottom and/or pore waters, which affect iodate concentrations in the water. We expect benthic foraminifera to record lower I/Ca at sites where an OMZ impinges on the seafloor [*Rue et al.*, 1997], and high I/Ca values at better oxygenated sites far below an OMZ (Figures 1a and 1b). The first core top study of infaunal and epifaunal benthic species living near an OMZ confirmed that I/Ca values correlate with bottom water [O_2] and that infaunal species (calcifying from pore waters) have lower I/Ca than epifaunal species [*Glock et al.*, 2014]. Without a local OMZ, the iodate concentration in modern oxygenated bottom water remains ~0.45 μM, due to the oceanic residence time of iodine of ~300 kyr [*Broecker and Peng*, 1982]. The concentration of iodate, a micronutrient, does not increase during the aging of deep waters [*Nakayama et al.*, 1989; *Waite et al.*, 2006]. This is probably due to the low I/C_{org} in plankton [*Elderfield and Truesdale*, 1980], and contrasts to the patterns of major nutrients in organic particles, such as nitrate and phosphate, and $\delta^{13}C$ in dissolved inorganic carbon (DIC). If the same mechanisms controlled iodine chemistry in the Paleogene, similar epifaunal benthic I/Ca values should be expected for coeval sites without a local OMZ, assuming that foraminiferal I/Ca values largely reflect seawater iodate levels [*Glock et al.*, 2014; *Zhou et al.*, 2014; *Lu et al.*, 2016].

1.3. Mn Oxides and Ce Anomalies as Redox Indicators

Mn is mostly delivered to the oceans as oxide coatings on particles by wind, river, or diffusion from shelf sediments [*Bender et al.*, 1977; *Calvert and Pedersen*, 1993]. Mn is scavenged throughout the oxic part of the water column and deposited on the seafloor mainly as Mn oxides in oxygenated bottom waters [*Bender et al.*, 1977; *Klinkhammer and Bender*, 1980], a process that may be biologically mediated [e.g., *Tebo et al.*, 2004]. Mn oxides are partially reduced to Mn^{2+} through microbial activity during early diagenesis of organic matter in the sediments, and the dissolved Mn^{2+} moves upward through diffusion and advection, forming an authigenic Mn oxide front in subsurface sediments at the oxic/suboxic boundary (Figures 1c and 1d) [*Froelich et al.*, 1979; *Klinkhammer and Bender*, 1980; *Chun et al.*, 2010]. As such, the presence of abundant Mn oxide in bulk sediments could suggest oxidative diagenetic alteration, and the absence of Mn oxide with the formation of Mn carbonate in the sediment indicates deoxygenation. Some authigenic Mn oxide is reduced when buried deeper in the sediment column [*Mangini et al.*, 2001]. As Mn^{2+} becomes more concentrated, authigenic Mn carbonate could precipitate, given sufficient alkalinity and DIC [*Neumann et al.*, 2002; *Schenau et al.*, 2002; *Pälike et al.*, 2014].

Cerium (Ce) is the only trivalent rare earth element (REE) that can be oxidized to the less soluble tetravalent form Ce(IV) under oxygenated conditions. In oxic seawater, Ce(IV) is preferentially sequestered into Mn-oxides and Mn-hydroxides [*Elderfield et al.*, 1981; *Bau et al.*, 1996; *Tachikawa et al.*, 1999]. When the concentrations of REEs are normalized to the average concentrations in shales, redox-driven scavenging of Ce produces seawater REE patterns with negative Ce anomalies, i.e., lower concentrations than predicted relative to the nearest REE neighbors lanthanum (La) and praseodymium (Pr). Different methods can be used to denote a Ce anomaly, such as normalizing Ce to Nd rather than Pr. The Ce anomaly in this study is quantified by the ratio of Ce/Ce*, where Ce is the measured concentration and Ce* is the predicted concentration as interpolated from La and Pr, as in the equation $Ce/Ce^* = 2\ (Ce/Ce_{shale})/(La/La_{shale} + Pr/Pr_{shale})$ [*De Baar et al.*, 1985]. REE concentrations in shales are from *Haskin and Haskin* [1966]. The Ce/Ce* value is around 0.1 for oxic seawater (i.e., negative anomaly) and approaches unity (i.e., 1.0) in low-oxygen environments. Mn-oxides and Mn-hydroxides have positive Ce anomalies [*Bau et al.*, 1996; *Ling et al.*, 2013]. Ce is mostly oxidized and adsorbed onto Mn(IV) particles in surface waters through biological activities; thus, the Ce anomaly value remains constant below OMZs, although O_2 concentration increases with depth in the water column [*Alibo and Nozaki*, 1999; *Ling et al.*, 2013]. In modern oceans, Ce/Ce* in the pore waters with oxic overlying bottom waters is generally below 0.5, whereas that in suboxic pore waters is between 0.5 and 1 (Figure 1e) [*Haley*

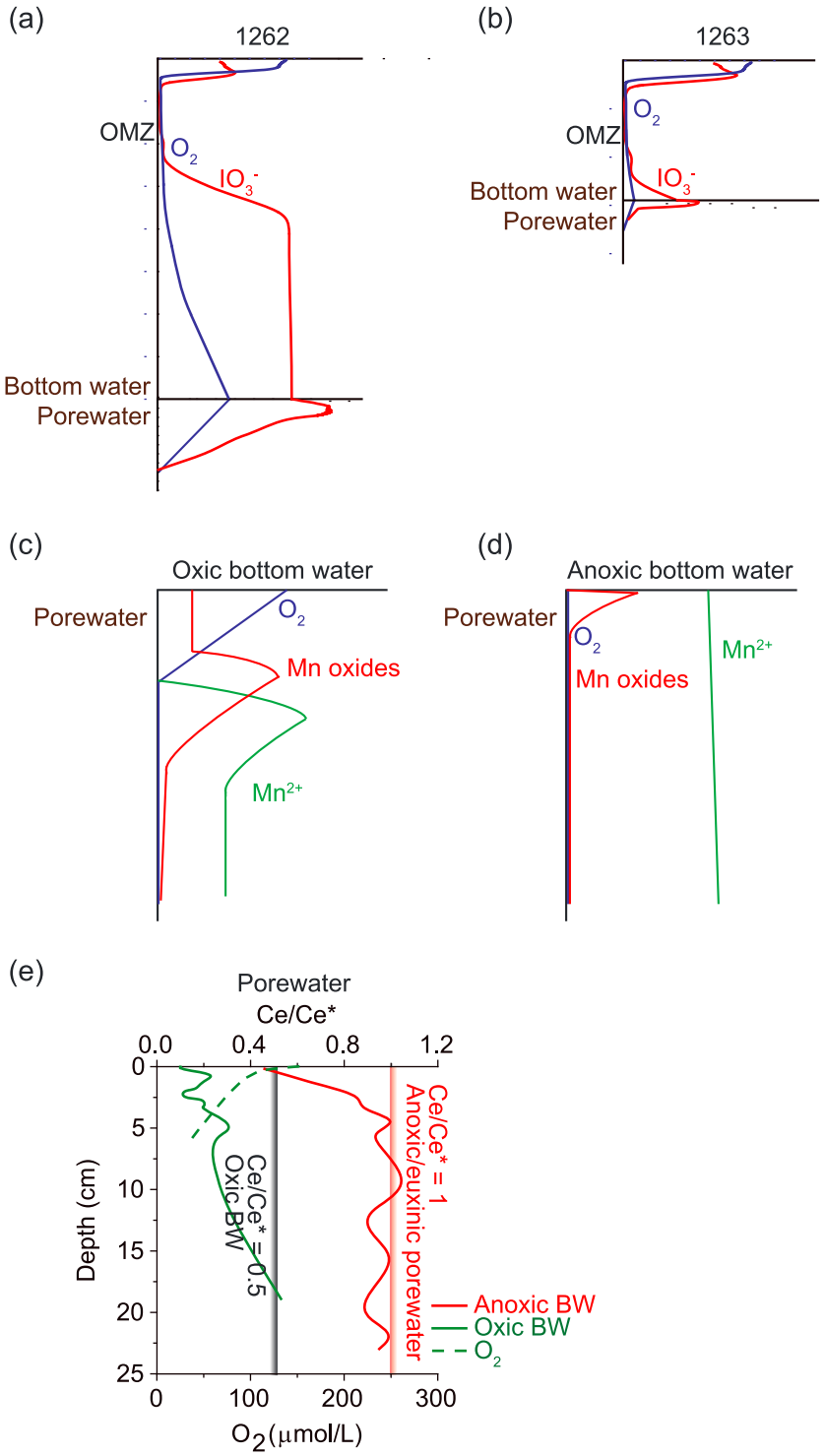

Figure 1. Expected iodate depth profiles in the water column and pore water for Sites (a) 1262 and (b) 1263, (c and d) Mn^{2+} and Mn oxides depth gradient, and (e) Ce/Ce* profile in pore water under different redox conditions. Data for Figures 1a and 1b are from *Rue et al.* [1997] and *Kennedy and Elderfield* [1987]. Figures 1c and 1d are modified from *Schenau et al.* [2002] and *Reitz et al.* [2006]. The red line in Figure 1e represents the Ce/Ce* trend in sta10, a California margin site; the solid green line denotes the Ce/Ce* record in MC64, a site from the Nazca Ridge off Peru; and the dashed green line is the dissolved O_2 concentration in pore water at the same site [*Haley et al.*, 2004]. The red bar in Figure 1d is defined as Ce/Ce* = 1, and the grey bar as Ce/Ce* = 0.5. Ce/Ce* values to the left of the grey bar are typical in oxic pore water, while values between the red and gray bars suggest suboxic pore water, as is shown in Figure 2.

et al., 2004]. REEs are rapidly incorporated into fish teeth during early diagenesis, while still in contact with seawater, exchanging with pore water during later burial at a much slower rate [*Kocsis et al.*, 2010; *Herwartz et al.*, 2011].

2. Sites and Methods

2.1. Study Sites

We generated benthic foraminiferal I/Ca records from four open ocean sites drilled by the Ocean Drilling Program (ODP): ODP Sites 1262 (paleodepth 3600 m) and 1263 (paleodepth 1500 m) on Walvis Ridge in the southeastern Atlantic Ocean, ODP Site 690 (paleodepth 1900 m) on Maud Rise (Weddell Sea) in the Southern Ocean, and ODP Site 738 on Kerguelen Plateau in the southern Indian Ocean [*Thomas*, 1990, 1998; *Zachos et al.*, 2004; *Winguth et al.*, 2012]. These sites provide the opportunity to show bottom water redox conditions at different water depths and allow comparison with Ce and Mn proxies. Combined with previous investigations into upper ocean redox conditions by measuring I/Ca in planktonic foraminiferal tests [*Zhou et al.*, 2014], this study may help in understanding the hydrography at these sites.

2.2. Foraminiferal I/Ca

We picked specimens from single species or genera of benthic foraminifera, i.e., the epifaunal *Nuttallides truempyi*, *Cibicidoides* spp. (mainly biconvex species with coarse pores on the evolute side, belonging to the *C. mundulus/praemundulus* group and *Cibicidoides eocaenus*), *Stensioeina beccariiformis*, and *Anomalinoides danica*; the shallow infaunal *Oridorsalis umbonatus*; and the deeper infaunal *Lenticulina* spp. (Table 1) [*Thomas and Shackleton*, 1996; *Katz et al.*, 2003]. Whether benthic foraminiferal species live infaunally or epifaunally is not well known. For many taxa the relationship between test morphology and microhabitat has not been observed but is extrapolated from data on other taxa and morphological similarities [e.g., *Jorissen et al.*, 2007]. In addition, many foraminifera move vertically through the sediment [e.g., *Rathburn and Corliss*, 1994; *Gooday and Rathburn*, 1999]. In one of the few studies evaluating the links between test morphology and microhabitat statistically, assignments for modern foraminifera were found to be accurate only about 75% of the time [*Buzas et al.*, 1993]. We thus mainly rely on stable isotope data to assign species to a dominantly infaunal or epifaunal status [*Thomas and Shackleton*, 1996; *Katz et al.*, 2003].

The specimens were crushed between two glass slides to open the chambers of each foraminifer, then cleaned following the Mg/Ca protocol in *Barker et al.* [2003]. Crushed foraminiferal shells were transferred to centrifuge tubes and put in an ultrasonic water bath to remove clays, before cleaning by NaOH-buffered H_2O_2 to remove organic material. The H_2O_2 solutions were then removed, and the specimens were rinsed with deionized water for 3 times.

The cleaned foraminiferal shells were dissolved in 3% (v/v) HNO_3 and mixed with a matrix, containing internal standards and buffered by tertiary amine. Iodine and calcium concentrations were then measured by inductively coupled plasma–mass spectrometer (ICP-MS) at Syracuse University. Calibration standards were freshly made for each batch of samples. The 1 ppb iodine signal was tuned to 80–120 kHz, with blank signal as low as 30 kHz. The reference material JCp-1 was measured repeatedly to maintain long-term accuracy [*Lu et al.*, 2010]. The standard deviation for each measurement of iodine and calcium is usually lower than 1%.

2.3. Fossil Fish Tooth REE Concentrations

Fossil fish teeth were hand-picked from the >150 μm size fraction of selected samples from a separate sample set than used for foraminiferal I/Ca. Fossil fish teeth samples consisted of two to five teeth each, ranging from 10 to 100 μg. Samples were sonicated in quartz distilled water and methanol to remove debris from surfaces and cavities, then treated with reductive and oxidative steps to remove oxides and organic matter, and weak acid steps [*Boyle*, 1981; *Boyle and Keigwin*, 1985; *Rosenthal et al.*, 1997]. Samples were then transferred into precleaned microcentrifuge tubes before and after the partial dissolution step. Cleaned fish teeth were weighed by using a microbalance and transferred into clean microcentrifuge tubes. The material was then dissolved in a dilute internal standard solution (2% HNO_3 containing indium, rhenium, and bismuth (In, Re, and Bi), used as internal standards) and measured on an element ICP-MS at the University of California at Santa Cruz or the University of South Carolina. Tuning and calibration were carried out with the guard electrode switched off to reduce oxide formation rates. This tended to produce lower signals, but counts per second were still remarkably high due to high concentrations of REE in fossil fish teeth. Silicate rock standards

Table 1. Average I/Ca and Standard Deviation (μmol/mol) for Each Foraminiferal Species at Each Site

		Epifaunal				Epifaunal/Attached to Raised Surfaces				Epifaunal		Epifaunal	Shallow Infaunal (0–4 cm)				Shallow to Deep Infaunal			
		N. truempyi				*Cibicidoides* spp.				*S. beccariiformis*		*A. danica*	*O. umbonatus*				*Lenticulina* spp.			
Site	Paleodepth (m)	Pre-CIE	±	CIE	±	Pre-CIE	±	CIE	±	Pre-CIE	±	Pre-CIE	Pre-CIE	±	CIE	±	Pre-CIE	±	CIE	±
738	1400	17.6	1.3	16.8	5.7															
690	1900	19.2	1.1	19.3	1.3					16.7		22.6			0.8		1.1	0.5		
1262	3600	26.2	3.3	27.2	6.4					14.4	4.2		8.4	3.2	4.7					
1263	1500	19.1	2.6	21.1	2.9	13.8	2.4	11.7	0.4	17.6	2.2		2.6	1.1	1.9	0.6	2.2	0.2	1.5	0.1

(AGV-2, W-2, BCR-2, DNC-1, BIR-1, and BHVO-2) were used to produce a calibration curve for REE concentrations. Matrix effects were examined in two ways. First, the silicate rock standard W-2 was doped with calcium and phosphorus to mimic expected concentrations in phosphate samples. Doped and undoped W-2, run as unknowns, did not show any measureable differences in REE concentrations. Second, a phosphate standard, the fossil bone composite [*Chavagnac et al.*, 2007], was run as an unknown by using the silicate rock-based calibration curve. Repeat measurements of the fossil bone composite yielded REE concentrations within 2–6% of values reported in *Chavagnac et al.* [2007] and showed an excellent fit with data compiled during the calibration of this standard [*Scher et al.*, 2011].

2.4. Model Projected Bottom Water O_2 Concentrations During the Late Paleocene

Bottom water oxygen concentrations for the late Paleocene were simulated in the fully coupled atmosphere-ocean general circulation model Community Climate System Model Version 3 (CCSM3) [*Collins et al.*, 2006] that includes a land surface and sea ice model [*Winguth et al.*, 2010, 2012]. CCSM3 has spectral horizontal resolution of T31, which uses a transform grid of ~3.75° × 3.75°, 26 vertically unevenly spaced terrain-following levels in the atmosphere, and a nominal 3° horizontal grid with 25 vertical layers in the ocean. The model was fully coupled and integrated for 2500 years. We used the oxygen simulation results in a ×4 CO_2 and a ×8 CO_2 scenario with prescribed pCO_2 of ×4 and ×8 preindustrial atmospheric levels (PAL) of 280 ppmv, respectively [*Winguth et al.*, 2012].

In addition, we used the "cGENIE" Earth system model [*Ridgwell et al.*, 2007], a 3-D dynamic ocean circulation model with simplified "energy and moisture" balance atmosphere [*Edwards and Marsh*, 2005], a representation of the biogeochemical cycling of elements and isotopes in the ocean [*Ridgwell et al.*, 2007] including that of ^{13}C [*Kirtland Turner and Ridgwell*, 2016]. Here we applied the early Eocene configuration of *Ridgwell and Schmidt* [2010], which assumed 834 ppm CO_2 in the atmosphere. The 10° longitude (and variable latitude) grid spacing is ~3 times on average coarser than in CCSM3, but the much shorter run-time enables us to explore a wide range of potential scenarios of past ocean circulation.

3. Results

We measured I/Ca at four open ocean sites in uppermost Paleocene and lowermost Eocene sediments, but with only few observations within the PETM (Figure 2). Benthic I/Ca data were plotted combined with $\delta^{13}C$ records for each site, showing the negative carbon isotope excursion (CIE) starting at 0 kyr, negative ages representing the late Paleocene (Figure 2). We generated *N. truempyi* (epifaunal) I/Ca records for all sites; other benthic species are not as commonly present. *Nuttallides truempyi*, however, is generally absent just after the onset of the PETM [*Foster et al.*, 2013].

Nuttallides truempyi I/Ca values at Site 1262 are generally higher than those at other sites, with average Paleocene I/Ca values of 26.2 μmol/mol, 19.1 at Site 1263, 19.2 at Site 690, and 17.6 at Site 738 (Table 1). I/Ca values of *N. truempyi* are generally higher than values of other epifaunal benthic species in the same sample interval. *Cibicidoides* spp. (epifaunal) and *S. beccariiformis* (epifaunal) have I/Ca values ranging from 10 to 20 μmol/mol at Sites 1262, 1263, and 690. At Site 1263, *N. truempyi* have consistently higher I/Ca values than *Cibicidoides* spp. (Figure 2), indicating higher iodate uptake efficiency in *N. truempyi*. Two I/Ca values of *A. danica* (epifaunal) are higher than those of *N. truempyi* at Site 690 (Figure 2). Among the four sites, we have only a few observations within the CIE, with values of epifaunal species slightly lower during the CIE

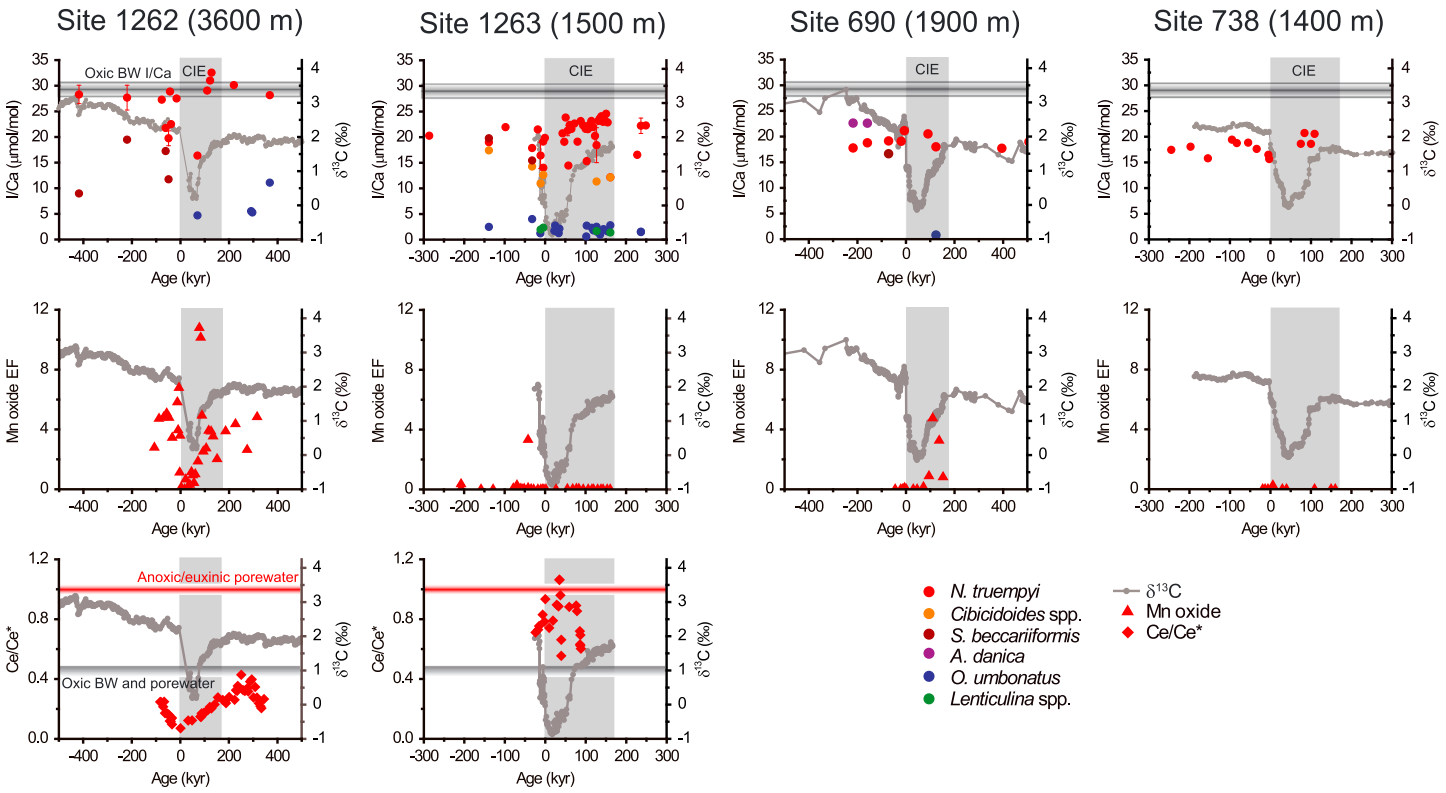

Figure 2. Benthic I/Ca, Mn oxide, and Ce/Ce* records for multiple open ocean sites, including ODP sites 1262 and 1263 on Walvis Ridge, Atlantic Ocean, ODP Site 690 in the Southern Ocean, and ODP Site 738 in Indian Ocean [*Chun et al.*, 2010]. The error bars are plotted for I/Ca data points when available. $\delta^{13}C$ record is plotted in every figure showing the CIE. The vertical gray bars indicate the temporal extent of the CIE. The horizontal gray bars in I/Ca plots represent the average I/Ca values in *N. truempyi* excluding those low values at Site 1262. The horizontal gray bars in Ce/Ce* plots are defined as Ce/Ce* = 1 and the red bars as Ce/Ce* = 0.5. Ce/Ce* values above the red bars represent anoxic/euxinic pore water, values between the gray and red bars suggest suboxic condition, and values below the grey bars indicate oxic pore water.

compared to pre-CIE at both Sites 1262 and 1263. However, data points from within the CIE recovery intervals at Sites 690 and 738 show values similar to those in the late Paleocene (Figure 2).

I/Ca values in *Oridorsalis umbonatus* and *Lenticulina* spp. are generally below 10 μmol/mol, considerably lower than in the epifaunal species (as expected), recording in situ pore water iodate levels. The *O. umbonatus* I/Ca values at Site 1262 are relatively higher (5–15 μmol/mol) than at Sites 1263 and 690, which are below 3 μmol/mol. The shallow infaunal species *O. umbonatus* has slightly higher values than the potentially deeper infaunal *Lenticulina* spp. at Site 1263. The I/Ca records of species from different habitats at the same time thus suggest that benthic foraminiferal tests indeed reflect iodate levels in the waters where the foraminiferal tests were calcified. At Site 1263, the only site from which I/Ca data for infaunal species within the CIE are available for a sufficient number of samples, the I/Ca values in infaunal taxa in the CIE do not differ significantly from background values.

The Mn oxide enrichment factors (EFs) were calculated from published Mn EF values in bulk sediment with and without reductive cleaning [*Chun et al.*, 2010; *Pälike et al.*, 2014]. Total concentrations of Mn were measured on a high-resolution ICP-MS [*Chun et al.*, 2010]. Bulk sediment Mn EF represents the sum of Mn oxides and $MnCO_3$, whereas the Mn EF measured after reductive cleaning reflects only $MnCO_3$. We calculated the difference between these two sets of EF values to denote the Mn oxide EF. Site 1262 is the only site with persistent Mn oxide preservation. Other sites generally do not show Mn oxides, probably indicating bottom water oxygen levels lower than that at Site 1262.

Fish teeth Ce/Ce* data are available for the two Walvis Ridge sites, showing contrasting values and patterns (Figure 2). All Ce/Ce* values are below 0.5 at the deeper Site 1262, decreasing from ~0.25 in the upper Paleocene to nearly 0 at the beginning of the CIE. The Ce/Ce* value rose from 0 to ~0.43 kyr, from 0 to

~250 kyr, then decreased to ~0.2 at ~350 kyr. The Ce/Ce* values at Site 1263 mostly scatter between 0.5 and 1 without a clear trend. The contrasting Ce/Ce* values at two Walvis Ridge sites confirm the presence of more oxygenated bottom waters at the deeper Site 1262.

Bottom water O_2 concentrations in CCSM3 (×4 CO_2) decrease from Site 1262 to Sites 690, 1263, and 738 (Figure 3a), with very low values of ~20–30 μmol/kg. Much higher bottom water O_2 concentrations (>150 μmol/kg) were simulated for all sites in the default configuration of cGENIE. Additional scenarios were evaluated in cGENIE, and the range of O_2 concentrations can be reduced to ~60–90 μmol/kg by adding fresh water at high southern latitudes, forcing the model to modify circulation patterns and decrease ocean ventilation in the regions where our sample sites were located.

4. Discussion

4.1. Vertical O_2 Gradient on Walvis Ridge

Today, iodate concentrations are nearly uniform in well-oxygenated intermediate to deep waters. Iodate gets depleted close to or within an OMZ or in anoxic bottom water only [e.g., *Wong and Brewer*, 1977; *Rue et al.*, 1997]. If these observations are applicable to the early Cenozoic, Site 1262, as the deepest site (paleo depth 3.6 km), is least likely to be affected by an OMZ, thus should have high O_2 and record high seawater iodate concentration. The *N. truempyi* I/Ca values are higher at Site 1262 than at all other studied sites. Most I/Ca values of *N. truempyi* at Site 1262 are around 26 μmol/mol, whereas the values are notably lower (~19 μmol/mol) at the nearby, shallower Site 1263 (paleodepth of 1.5 km; Figure 2 and Table 1). If the difference in *N. truempyi* I/Ca values between these two Walvis Ridge sites was mostly driven by bottom water iodate concentrations, then the shallower Site 1263 was closer to an OMZ.

Such an interpretation is consistent with the reported Mn speciation data. Site 1262 is the only site that persistently preserved Mn-oxides, with Mn EFs as high as 11, and the Mn trend follows the $\delta^{13}C$ record, exhibiting lowest values at the beginning of the CIE (Figure 2). The lack of Mn oxides (as seen by the lack of micronodules) at other sites (Figure 2) most likely can be explained by the presence of low bottom water O_2 and negligible O_2 penetration into pore water, preventing the growth of diagenetic Mn oxides. Most of the Mn oxide EFs at Site 1263 are close to 0, except for one data point at -42.1 kyr (Figure 2) [*Chun et al.*, 2010; *Pälike et al.*, 2014]. Fish teeth Ce anomaly values (<0.5) indicate pore water oxygen penetration at the deepest Site 1262 before, during, and after the CIE. The Ce anomaly at Site 1263 indicates low bottom water oxygen. Epi-benthic I/Ca, Mn speciation and Ce anomaly are three independent redox proxies with different geochemical controls. The excellent consistency among these proxies at the Walvis Ridge sites strongly indicates the presence of an OMZ at intermediate depth, whereas bottom water at the deeper Site 1262 must have been well oxygenated. Currently, none of these proxies is yet capable of providing a robust, quantitative estimate of dissolved O_2 concentrations. In addition, there is an interval without carbonate (thus without foraminifera) across the PETM at Site 1262, where we have no I/Ca data. Micronodules with an unusual Mn-oxide (jianshuiite) in this interval indicate that a transient period of declining pH and Eh conditions may have occurred even at this deep site [*Post et al.*, 2016].

In addition to seawater iodine concentration and local-regional OMZ presence, iodine speciation changes in shallow pore waters influence I/Ca values in infaunal foraminifera. Iodate concentrations in the pore water of marine sediments commonly increase from the oxygenated sediment-water interface toward the shallow subsurface, then decrease to zero at the oxic/anoxic boundary [*Kennedy and Elderfield*, 1987], an early diagenetic feature similar to solid phase manganese enrichment (Figures 1a–1d). Lower bottom water O_2 concentrations may partially limit the pore water O_2 penetration beneath the sediment-water interface, leading to a steeper iodate depth gradient (Figures 1a and 1b). Thus, infaunal benthic foraminifera are expected to record low I/Ca values under poorly oxygenated bottom water, integrating the steep pore water iodate gradient in a narrow habitat. At well-oxygenated sites, infaunal I/Ca values may heavily depend on calcification depth. Shallow infaunal species living close to the pore water iodate peak may record high I/Ca values, but deep infaunal species living near the anoxic boundary would have low I/Ca, even with high bottom water O_2 (Figures 1a and 1b). Regardless of additional complications such as changing depth habitat [e.g., *Jorissen et al.*, 2007; *Gooday and Rathburn*, 1999], infaunal species are more likely to record higher I/Ca at well-oxygenated sites than at O_2-depleted sites. I/Ca in Eocene *O. umbonatus* is ~10 μmol/mol at Site 1262, compared to

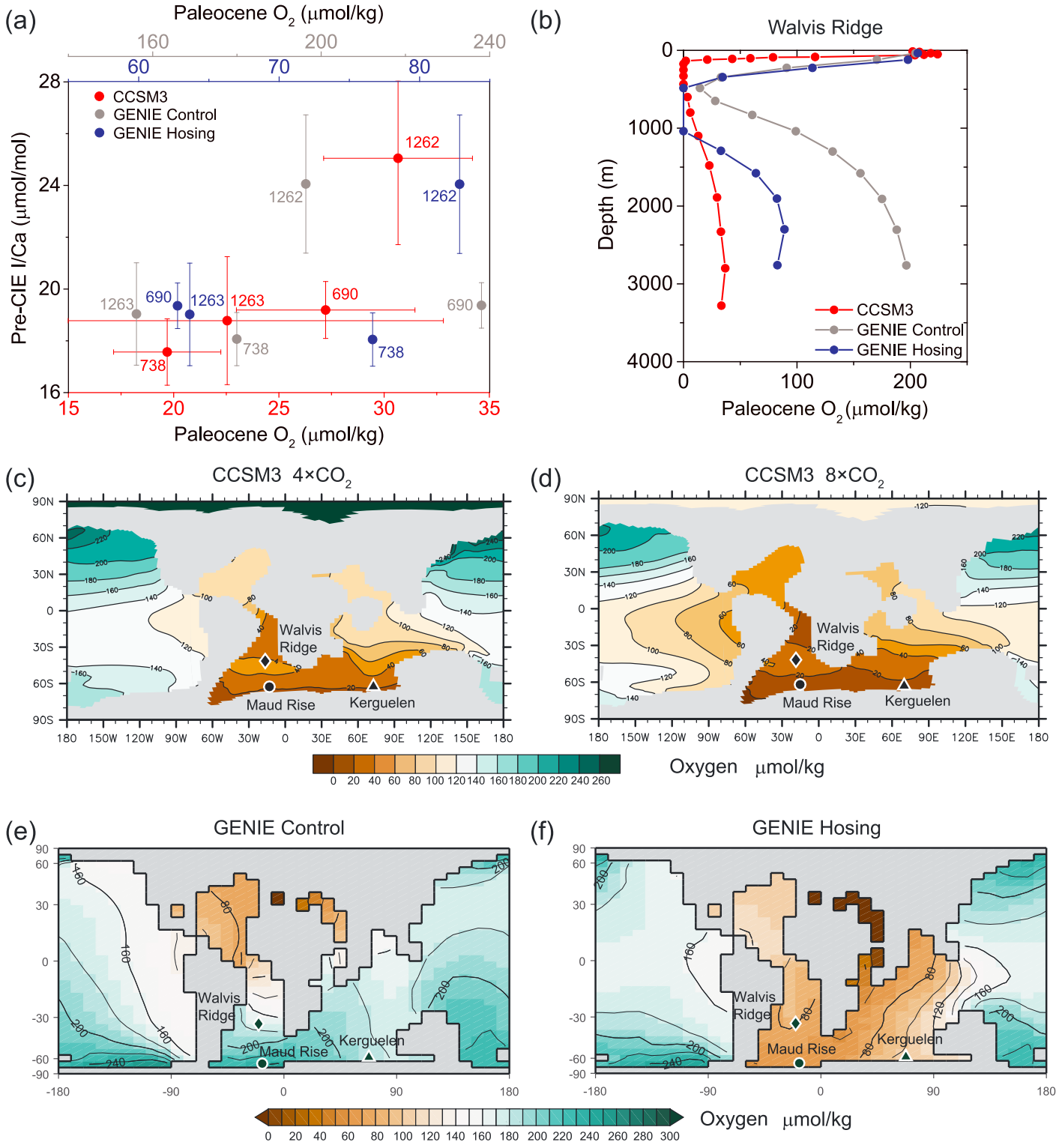

Figure 3. (a) Pre-CIE average *N. truempyi* I/Ca values at each site are plotted against modeled bottom water O_2 in the late Paleocene by CCSM3 [*Winguth et al.*, 2012] and two simulations by cGENIE (i.e., control and hosing). The error bars of pre-CIE I/Ca values stand for the standard deviation of those values, and those of modeled bottom water O_2 by CCSM3 represent the O_2 levels approximately 500 m above or below the paleodepth of each site. (b) Modeled O_2 concentrations through the water column on Walvis Ridge in the late Paleocene by CCSM3 and cGENIE. (c and d) Modeled global seafloor oxygen levels with atmospheric pCO_2 of ×4 and ×8 PAL in the late Paleocene by CCSM3. (e) Simulated global seawater O_2 levels at ~2000 m by cGENIE under the condition of ×3 CO_2 in the default late Paleocene (control experiment), with the symbols of diamond, circle, and triangle representing site locations of 1262 and 1263, 690, and 738, respectively. (f) Same settings as Figure 3e except adding fresh water at high-latitude South Atlantic Ocean (hosing experiment).

~3 μmol/mol at Site 1263 (Figure 2), most likely due to lower bottom water O_2 at Site 1263, consistent with the conclusions drawn from epi-faunal I/Ca, Mn, and Ce data.

4.2. Possible Widespread O_2 Depletion at Intermediate Depths

Norris et al. [2013] suggested that ocean oxygenation may have been relatively poor during greenhouse climates, based on BFOI only, which is not considered a reliable proxy [e.g., *Jorissen et al.*, 2007]. It is challenging to use biological or geochemical proxies to make even semiquantitative estimates of bottom water dissolved O_2 concentrations at a specific site, beyond general assessment of relatively more oxic or more reducing conditions. The available Mn data suggest that oxygenation of bottom waters was low during the PETM in the Atlantic Ocean but high across the late Paleocene-early Eocene in the Pacific Ocean [*Pälike et al.*, 2014].

If the relatively low Paleocene I/Ca in *N. truempyi* at Site 1263 (compared to Site 1262) indeed indicates the influence of an OMZ, very similar *N. truempyi* I/Ca values at Sites 690 and 738 (Table 1) may indicate widespread O_2 depletion at the intermediate depths of high-latitude South Atlantic and Southern Indian Oceans, in agreement with *Pälike et al.* [2014]. The Mn oxide EFs are almost all zeros at Site 690, except for a peak of 4.75 near 100 kyr, which suggests suboxic bottom waters with the peak in uranium EF occurring at the same time with peak Mn EF values [*Pälike et al.*, 2014]. Mn oxide EF values at Site 738 are all near zero [*Pälike et al.*, 2014]. In addition, I/Ca values in *O. umbonatus* at Site 690 are also comparable to those at Site 1263, much lower than the *O. umbonatus* values at Site 1262, further supporting other proxy data. However, to better constrain the bottom water redox conditions at Sites 690 and 738, a multiproxy comparison for extended depth transects is needed.

4.3. CIE Versus Non-CIE

Due to the lack of epifaunal specimens in the CIE interval, we cannot reconstruct detailed changes in oxygenation during the PETM. I/Ca values in *N. truempyi* do not follow the benthic $\delta^{13}C$ trend at any site, indicating that the seafloor deoxygenation was not fully synchronous with the global carbon perturbation, thus warming. Relatively, lower I/Ca values seem to appear during short intervals, which appear to occur more frequently close to or within the CIE interval on Walvis Ridge, suggesting that exacerbated deoxygenation may have occurred in short pulses. These records, however, may have been influenced by bioturbation, so that the short peaks may not reflect seafloor conditions, but vertical distribution of foraminiferal populations affected to different extents by mixing of PETM and non-PETM specimens. Such bioturbation is commonly seen in high-resolution stable isotope, single specimen data [e.g., *Thomas et al.*, 2002]. Most *N. truempyi* I/Ca values during the recovery stage of the CIE are very similar to those of non-CIE intervals (Figure 2 and Table 1), possibly suggesting that carbonate dissolution and seawater pH might not have a dominant effect on *N. truempyi* I/Ca. This should be further investigated.

4.4. Seawater Iodine Concentrations

The bottom water iodate concentration at Site 1263, which was near an OMZ, should have been lower than that at oxygenated sites in the late Paleocene. In modern oceans, iodate accounts for over 99% of total iodine in the bottom water of deep oceans [e.g., *Tsunogai*, 1971], recorded as high I/Ca values in benthic foraminifera. Assuming a similar mechanism in the late Paleocene, the I/Ca values in benthic foraminifera from oxygenated bottom water, as recorded at Site 1262, should reflect the total iodine concentration in seawater at that time. The majority of the I/Ca values in late Paleocene epifaunal species (*Cibicidoides* spp. and *N. truempyi*) are the highest among all I/Ca values reported in foraminifera and bulk carbonate [e.g., *Zhou et al.*, 2014, 2015; *Glock et al.*, 2014]. Considering potential vital effects from different epifaunal species, we compared *Cibicidoides* spp. I/Ca values, from modern oceans and from the late Paleocene. *Cibicidoides* spp. at Site 1263, living in O_2-depleted bottom water with low iodate, have I/Ca values higher than those (~10 μmol/mol) in core-top samples (recent-late Holocene specimens) from North and South Atlantic, with $O_2 > 200$ μmol/kg.

This suggests that the total iodine concentration in the late Paleocene-early Eocene was higher than it is in modern-Holocene seawater. These I/Ca records are not long enough to show whether such high iodine concentrations lasted for a few million years around the Paleocene-Eocene boundary or were present for a more substantial portion of the early Cenozoic. Sustaining high seawater iodine concentrations over tens of millions of years may involve complex earth system changes, but shorter perturbations to the iodine cycle

around the PETM could have been achieved by magma interactions with organic-rich (and iodine-rich) basin sediments [*Storey et al.*, 2007]. Lower organic carbon burial theoretically could increase total iodine concentration in seawater, although no convincing evidence was found for iodine drawdown during Oceanic Anoxic Events, characterized by enhanced organic carbon burial [*Zhou et al.*, 2015]. Pore waters in modern gas hydration fields are almost always enriched in iodine, orders of magnitude above seawater concentration [*Lu et al.*, 2008, 2011]. Box models may be able to evaluate the importance of pore water iodine release with methane during the PETM, but a peak of higher I/Ca during the CIE is not evident in our records.

4.5. Data-Model Comparison

Proxy data from our sites in the South Atlantic and Southern Indian Ocean indicate that in the late Paleocene OMZs were widespread and thick, extending down to 1.5–2 km in the water column. Planktonic foraminiferal I/Ca values suggest that an OMZ was present at multiple open ocean sites during the PETM [*Zhou et al.*, 2014]. To test this pattern, Paleocene average *N. truempyi* I/Ca values from each site were plotted against the bottom water O_2 concentrations modeled in CCSM3 (×4 CO_2) and two experiments in cGENIE (Figure 3).

The state of past circulation in the late Paleocene is highly uncertain [e.g., *Nunes and Norris*, 2006; *Zeebe and Zachos*, 2007; *Lunt et al.*, 2010, 2012; *Alexander et al.*, 2015]. *Lunt et al.* [2010] demonstrate that an atmospheric CO_2 and surface warming threshold could exist, beyond which any further CO_2 rise and surface warming leads to a disproportionately larger increase in temperature in the intermediate waters than in the deep ocean. This kind of intermediate depth warming would reduce O_2 solubility, and the integrated remineralization of organic matter along its circulation pathway will also affect the local value of $[O_2]$.

First, comparing model results with I/Ca values, Site 1263 was located close to an OMZ and had lower bottom water dissolved O_2 concentrations than the deeper Site 1262 in all three simulations (Figures 3a and 3b). The highest average I/Ca value corresponds to the highest modeled $[O_2]$ (Site 1262) in CCSM3, whereas the I/Ca and simulated dissolved O_2 concentrations are much lower at the other three sites. The pattern of bottom water dissolved $[O_2]$ projected by CCSM3 is consistent with our measured gradients in I/Ca (Figure 3a). However, the modeled bottom water $[O_2]$ are almost 1 order of magnitude lower than modern-day values at the same sites, because of lower solubility and ocean ventilation, especially at high southern latitudes. The deepest location (Site 1262) in particular would be relatively well ventilated under modern conditions, whereas CCSM3 predicts a less ventilated state with a dissolved oxygen concentration of only ~30 μmol/kg in the simulation. We do not know the threshold $[O_2]$ beneath which *N. truempyi* I/Ca would start to decrease. The preservation of Mn oxide, as observed at Site 1262, may require a dissolved $[O_2]$ of ~60–150 μmol/kg in bottom water [*Shaw et al.*, 1990], but the proxy data in this study cannot be reliably converted to dissolved O_2 values to compare with CCSM3 simulations.

In the control ×3 CO_2 scenario, cGENIE [*Kirtland Turner and Ridgwell*, 2016] predicts bottom water $[O_2]$ to be $>$ ~150 μmol/kg at Site 1262, with an overlying OMZ and hence depleted values at Site 1263 (Figure 3b). However, the N-S Atlantic basinal O_2 gradient in cGENIE is opposite to that in CCSM3 at intermediate depths (e.g., ~2 km; Figure 3e). High bottom water O_2 concentrations simulated for Sites 690 and 738 associated with their proximity to sites of deepwater formation in the default configuration of cGENIE are not supported by the proxy data (e.g., I/Ca and Mn) at these two sites. In additional experiments (not shown) in which *c*GENIE was spun up at higher assumed atmospheric pCO_2, even intense greenhouse conditions of ×8 and ×16 CO_2 did not reverse this N-S Atlantic O_2 pattern at intermediate depths.

We hence explored whether alternative but more prescribed scenarios of large-scale ocean circulation could produce O_2 patterns and concentrations consistent with proxy data. We found that we were able to generate a more CCSM3-like O_2 pattern which better correlated with epi-benthic I/Ca at Sites 690 and 738 (Figure 3d), by applying a fresh water forcing (hosing)—analogous to Atlantic Meridional Overturning Circulation "shutdown" experiments for the last glacial and deglacial [e.g., *Chikamoto et al.*, 2008], and hence slightly different to the zonal E-P modification applied in the classic Paleogene paleo-ocean circulation experiment of *Bice and Marotzke* [2001]. We do not suggest that such fresh water run off patterns necessarily occurred—we simply use this methodological device to force the model to decrease ocean ventilation at the highest southern latitudes. In comparing $\delta^{13}C$-derived patterns of circulation with I/Ca values, however, we note that Paleocene bottom water DIC $\delta^{13}C$ values simulated for our sites in the "hosing" experiment show a less significant correlation with measured benthic $\delta^{13}C$ as compared to the default Paleocene simulation. In other words, while

we can improve the correlation between modeled dissolved oxygen and I/Ca, we degrade the correspondence between modeled bottom water DIC $\delta^{13}C$ and measured benthic $\delta^{13}C$. The effect of stratification and warming on O_2 distribution needs to be better calibrated in the model. Future experiments may also explore additional scenarios (e.g., export production, nutrient, and remineralization depth) and eventually aim at reconciling both O_2 patterns and O_2 concentrations with a full suite of proxy data (e.g., I/Ca, Mn, Ce anomaly, and $\delta^{13}C$).

5. Conclusion

Uppermost Paleocene-lowermost Eocene benthic foraminiferal I/Ca records at open ocean sites suggest that benthic I/Ca can be used as bottom water (epifaunal) and pore water (infaunal) redox proxies, although on these time scales other factors (e.g., seawater total iodine) should also be considered. The comparison of benthic I/Ca with Mn oxide EF, Ce anomaly, and climate models suggests that waters at the deepest Site 1262 on Walvis Ridge were most oxygenated in the late Paleocene-early Eocene. Bottom waters at intermediate depths were likely affected by OMZs in the South Atlantic and Southern Indian Ocean, with lower oxygen concentrations during this period of Greenhouse climate than in today's oceans. The *Cibicidoides* spp. I/Ca values at OMZ-influenced Site 1263 are higher than those in modern well-oxygenated open ocean locations, suggesting higher total iodine concentrations in seawater in the late Paleocene than at present. CCSM3 and cGENIE are both capable of simulating Paleocene oxygen depletion at the intermediate depth, but a fully reconciled data-model comparison is complex because of the approximations made in both the paleoproxies and modeling.

Acknowledgments

Z.L. and X.Z. thank NSF-OCE 1232620 and a collaborative project with NSF-OCE 1232413 to E.T. Z.L. and R.E.M.R. were supported by the Natural Environment Research Council NE/E018432/1 during the initial development of the I/Ca proxy. B.H. is supported by the UK Natural Environment Research Council (NERC) grant NE/I020563/1. A.W. is supported by NSF-OCE 1536630. The manuscript was greatly improved by suggestions from one anonymous reviewer, Anthony Rathburn, and Associate Editor Baerbel Hoenisch. This research used samples provided by the International Ocean Discovery Program (IODP). IODP is sponsored by the U.S. National Science Foundation and participating countries under management of the Joint Oceanographic Institutions. I/Ca data are available in the supporting information.

References

Alegret, L., S. Ortiz, I. Arenillas, and E. Molina (2010), What happens when the ocean is overheated? The foraminiferal response across the Paleocene-Eocene Thermal Maximum at the Alamedilla section (Spain), *Geol. Soc. Am. Bull.*, *122*, 1616–1624.

Alexander, K., J. K. Meissner, and T. J. Bralower (2015), Sudden spreading of corrosive bottom water during the Palaeocene–Eocene Thermal Maximum, *Nat. Geosci.*, *8*, 458–461, doi:10.1038/ngeo2430.

Alibo, D. S., and Y. Nozaki (1999), Rare earth elements in seawater, particle association, shale-normalization, and Ce oxidation, *Geochim. Cosmochim. Acta*, *63*(3–4), 363–372, doi:10.1016/S0016-7037(98)00279-8.

Barker, S., M. Greaves, and H. Elderfield (2003), A study of cleaning procedures used for foraminiferal Mg/Ca paleothermometry, *Geochem. Geophys. Geosyst.*, *4*(9), 8407, doi:10.1029/2003GC000559.

Bau, M., A. Koschinsky, P. Dulski, and J. R. Hein (1996), Comparison of the partitioning behaviours of yttrium, rare earth elements, and titanium between hydrogenetic marine ferromanganese crusts and seawater, *Geochim. Cosmochim. Acta*, *60*(10), 1709–1725.

Bender, M. L., G. P. Klinkhammer, and D. W. Spencer (1977), Manganese in seawater and the marine manganese balance, *Deep Sea Res.*, *24*(9), 799–812, doi:10.1016/0146-6291(77)90473-8.

Bice, K. L., and J. Marotzke (2001), Numerical evidence against reversed thermohaline circulation in the warm Paleocene/Eocene ocean, *J. Geophys. Res.*, *106*, 11,529–11,542, doi:10.1029/2000JC000561.

Bolle, M.-P., A. Pardo, K.-U. Hinrichs, T. Adatte, K. Von Salis, S. Burns, G. Keller, and N. Muzylev (2000), The Paleocene-Eocene transition in the marginal northeastern Tethys (Kazakhstan and Uzbekistan), *Int. J. Earth Sci.*, *89*(2), 390–414, doi:10.1007/s005310000092.

Boscolo-Galazzo, F., E. Thomas, M. Pagani, C. Warren, V. Luciani, and L. Giusberti (2014), The Middle Eocene Climatic Optimum (MECO): A multiproxy record of paleoceanographic changes in the South-east Atlantic (ODP Site 1263, Walvis Ridge), *Paleoceanography*, *29*, 1143–1161, doi:10.1002/2014PA002670.

Boyle, E. A. (1981), Cadmium, zinc, copper, and barium in foraminifera tests, *Earth Planet. Sci. Lett.*, *53*(1), 11–35, doi:10.1016/0012-821X(81)90022-4.

Boyle, E. A., and L. D. Keigwin (1985), Comparison of Atlantic and Pacific paleochemical records for the last 215,000 years: Changes in deep ocean circulation and chemical inventories, *Earth Planet. Sci. Lett.*, *76*(1–2), 135–150, doi:10.1016/0012-821X(85)90154-2.

Broecker, W. S., and H. T. Peng (1982), *Tracers in the Sea*, Lamont-Doherty Geol. Observatory, New York.

Buzas, M. A., S. J. Culver, and F. J. Jorissen (1993), A statistical evaluation of the microhabitats of living (stained) infaunal benthic foraminifera, *Mar. Micropaleontol.*, *29*, 73–76.

Calvert, S. E., and T. F. Pedersen (1993), Geochemistry of recent oxic and anoxic marine-sediments: Implications for the geological record, *Mar. Geol.*, *113*(1–2), 67–88, doi:10.1016/0025-3227(93)90150-t.

Canudo, J., G. Keller, E. Molina, and N. Ortiz (1995), Planktic foraminiferal turnover and δ13C isotopes across the Paleocene-Eocene transition at Caravaca and Zumaya, Spain, *Palaeogeogr. Palaeoclimatol. Palaeoecol.*, *114*(1), 75–100, doi:10.1016/0031-0182(95)00073-U.

Chavagnac, V., et al. (2007), Towards the development of a fossil bone geochemical standard: An inter-laboratory study, *Anal. Chim. Acta*, *599*(2), 177–190, doi:10.1016/j.aca.2007.08.015.

Chikamoto, M. O., K. Matsumoto, and A. Ridgwell (2008), Response of deep-sea CaCO3 sedimentation to Atlantic meridional overturning circulation shutdown, *J. Geophys. Res.*, *113*, G03017, doi:10.1029/2007JG000669.

Chun, C. O. J., M. L. Delaney, and J. C. Zachos (2010), Paleoredox changes across the Paleocene-Eocene Thermal Maximum, Walvis Ridge (ODP Sites 1262, 1263, and 1266): Evidence from Mn and U enrichment factors, *Paleoceanography*, *25*, PA4202, doi:10.1029/2009PA001861.

Collins, W. D., et al. (2006), The Community Climate System Model version 3 (CCSM3), *J. Clim.*, *19*(11), 2122–2143, doi:10.1175/JCLI-D-11-00290.1.

De Baar, H. J. W., M. P. Bacon, P. G. Brewer, and K. W. Bruland (1985), Rare earth elements in the Pacific and Atlantic Oceans, *Geochim. Cosmochim. Acta*, *49*(9), 1943–1959, doi:10.1016/0016-7037(85)90089-4.

Deutsch, C., et al. (2014), Centennial changes in North Pacific anoxia linked to tropical trade winds, *Science*, *345*(6197), 665–668, doi:10.1126/science.1252332.

Dickson, A. J., A. S. Cohen, and A. L. Coe (2012), Seawater oxygenation during the Paleocene-Eocene Thermal Maximum, *Geology*, *40*(7), 639–642, doi:10.1130/g32977.1.
Dickson, A. J., R. L. Rees-Owen, C. März, A. L. Coe, A. S. Cohen, R. D. Pancost, K. Taylor, and E. Shcherbinina (2014), The spread of marine anoxia on the northern Tethys margin during the Paleocene-Eocene Thermal Maximum, *Paleoceanography*, *29*, 471–488, doi:10.1002/2014PA002629.
Dunkley Jones, T., D. J. Lunt, D. N. Schmidt, A. Ridgwell, A. Sluijs, P. J. Valdes, and M. Maslin (2013), Climate model and proxy data constraints on ocean warming across the Paleocene–Eocene Thermal Maximum, *Earth Sci. Rev.*, *125*, 123–145.
Edwards, N. R., and R. Marsh (2005), Uncertainties due to transport-parameter sensitivity in an efficient 3-D ocean-climate model, *Clim. Dyn.*, *24*(4), 415–433, doi:10.1007/s00382-004-0508-8.
Elderfield, H., and V. W. Truesdale (1980), On the biophilic nature of iodine in seawater, *Earth Planet. Sci. Lett.*, *50*(1), 105–114.
Elderfield, H., C. Hawkesworth, M. Greaves, and S. Calvert (1981), Rare earth element geochemistry of oceanic ferromanganese nodules and associated sediments, *Geochim. Cosmochim. Acta*, *45*(4), 513–528, doi:10.1016/0016-7037(81)90184-8.
Falkowski, P. G., et al. (2011), Ocean deoxygenation: Past, present and future, *Eos Trans. AGU*, *92*, 409–410, doi:10.1029/2011EO460001.
Foster, L. C., D. N. Schmidt, E. Thomas, S. Arndt, and A. Ridgwell (2013), Surviving rapid climate change in the deep-sea during the Paleogene hyperthermals, *Proc. Natl. Acad. Sci. U.S.A.*, *110*, 9273–9276, doi:10.1073/pnas.1300579110.
Froelich, P. N., G. P. Klinkhammer, M. L. Bender, N. A. Luedtke, G. R. Heath, D. Cullen, P. Dauphin, D. Hammond, B. Hartman, and V. Maynard (1979), Early oxidation of organic-matter in pelagic sediments of the Eastern Equatorial Atlantic - suboxic diagenesis, *Geochim. Cosmochim. Acta*, *43*(7), 1075–1090.
Gavrilov, Y. O., E. Shcherbinina, and H. Oberhaensli (2003), Paleocene-Eocene boundary events in the northeastern peri-Tethys, in *Causes and Consequences of Globally Warm Climates of the Paleogene*, *Spec. Pap.*, vol. 369, edited by S. Wing et al., Geol. Soc. of Am., Boulder, Colo.
Giusberti, L., F. Boscolo-Galazzo, and E. Thomas (2016), Variability in climate and productivity during the Paleocene-Eocene Thermal Maximum in the western Tethys (Forada section), *Clim. Past*, *12*, 213–240, doi:10.5194/cp-12-213-2016.
Glock, N., V. Liebetrau, and A. Eisenhauer (2014), I/Ca ratios in benthic foraminifera from the Peruvian oxygen minimum zone: Analytical methodology and evaluation as a proxy for redox conditions, *Biogeosciences*, *11*(23), 7077–7095, doi:10.5194/bg-11-7077-2014.
Gooday, A. J. (2003), Benthic foraminifera (Protista) as tools in deep-water palaeoceanography: A review of environmental influences on faunal characteristics, *Adv. Mar. Biol.*, *46*, 1–90, doi:10.1017/CBO9781107415324.004.
Gooday, A. J., and A. E. Rathburn (1999), Temporal variability in living deep-sea benthic foraminifera: A review, *Earth Sci. Rev.*, *46*, 187–212.
Haley, B. a., G. P. Klinkhammer, and J. McManus (2004), Rare earth elements in pore waters of marine sediments, *Geochim. Cosmochim. Acta*, *68*(6), 1265–1279, doi:10.1016/j.gca.2003.09.012.
Haskin, M. A., L. A. Haskin (1966), Rare earths in European shales: a redetermination, *Science*, *154*, 507–509.
Helm, K. P., N. L. Bindoff, and J. A. Church (2011), Observed decreases in oxygen content of the global ocean, *Geophys. Res. Lett.*, *38*, L23602, doi:10.1029/2011GL049513.
Herwartz, D., T. Tütken, C. Münker, K. P. Jochum, B. Stoll, and P. M. Sander (2011), Timescales and mechanisms of REE and Hf uptake in fossil bones, *Geochim. Cosmochim. Acta*, *75*(1), 82–105, doi:10.1016/j.gca.2010.09.036.
Jenkyns, H. C. (2010), Geochemistry of oceanic anoxic events, *Geochem. Geophys. Geosyst.*, *11*, Q03004, doi:10.1029/2009GC002788.
John, E. H., J. D. Wilson, P. N. Pearson, and A. Ridgwell (2014), Temperature-dependent remineralization and carbon cycling in the warm Eocene oceans, *Palaeogeogr. Palaeoclimatol. Palaeoecol.*, *413*, 158–166, doi:10.1016/j.palaeo.2014.05.019.
Jorissen, F. J., C. Fontanier, and E. Thomas (2007), Paleoceanographical proxies based on deep-sea benthic foraminiferal assemblage characteristics, in *Proxies in Late Cenozoic Paleoceanography: Part 2: Biological Tracers and Biomarkers*, edited by C. Hillaire-Marcel and A. de Vernal, pp. 263–326, Elsevier, Amsterdam, Netherlands.
Kaiho, K. (1994), Benthic foraminiferal dissolved-oxygen index and dissolved-oxygen levels in the modern ocean, *Geology*, *22*(8), 719–722, doi:10.1130/0091-7613(1994)022<0719:BFDOIA>2.3.CO.
Kaiho, K., et al. (1996), Latest Paleocene benthic foraminiferal extinction and environmental changes at Tawanui, New Zealand, *Paleoceanography*, *11*, 447–465, doi:10.1029/96PA01021.
Katz, M. E., J. D. Wright, D. R. Katz, K. G. Miller, D. K. Pak, N. J. Shackleton, and E. Thomas (2003), Early Cenozoic benthic foraminiferal isotopes: species reliability and interspecies correction factors, *Paleoceanography*, *18*(2), 1024, doi:10.1029/2002PA000798.
Keeling, R. F., A. Kortzinger, and N. Gruber (2010), Ocean deoxygenation in a warming world, *Annu. Rev. Mar. Sci.*, *2*, 199–229, doi:10.1146/annurev.marine.010908.163855.
Kennedy, H. A., and H. Elderfield (1987), Iodine diagenesis in pelagic deep-sea sediments, *Geochim. Cosmochim. Acta*, *51*(9), 2489–2504.
Kennett, J. P., and L. D. Stott (1991), Abrupt deep-sea warming, palaeoceanographic changes and benthic extinctions at the end of the Palaeocene, *Nature*, *353*(6341), 225–229, doi:10.1038/353225a0.
Kirtland Turner, S., and A. Ridgwell (2016), Development of a novel empirical framework for interpreting geological carbon isotope excursions, with implications for the rate of carbon injection across the PETM, *Earth Planet. Sci. Lett.*, *435*, 1–13, doi:10.1016/j.epsl.2015.11.027.
Klinkhammer, G. P., and M. L. Bender (1980), The distribution of manganese in the Pacific Ocean, *Earth Planet. Sci. Lett.*, *46*(3), 361–384, doi:10.1016/0012-821X(80)90051-5.
Kocsis, L., C. N. Trueman, and M. R. Palmer (2010), Protracted diagenetic alteration of REE contents in fossil bioapatites: Direct evidence from Lu–Hf isotope systematics, *Geochim. Cosmochim. Acta*, *74*(21), 6077–6092, doi:10.1016/j.gca.2010.08.007.
Ling, H. F., X. Chen, D. Li, D. Wang, G. a. Shields-Zhou, and M. Zhu (2013), Cerium anomaly variations in Ediacaran-earliest Cambrian carbonates from the Yangtze Gorges area, South China: Implications for oxygenation of coeval shallow seawater, *Precambrian Res.*, *225*, 110–127, doi:10.1016/j.precamres.2011.10.011.
Lippert, P. C., and J. C. Zachos (2007), A biogenic origin for anomalous fine-grained magnetic material at the Paleocene-Eocene boundary at Wilson Lake, New Jersey, *Paleoceanography*, *22*, PA4104, doi:10.1029/2007PA001471.
Lu, Z., C. Hensen, U. Fehn, and K. Wallmann (2008), Halogen and 129I systematics in gas hydrate fields at the northern Cascadia margin (IODP Expedition 311): Insights from numerical modeling, *Geochem. Geophys. Geosyst.*, *9*, Q10006, doi:10.1029/2008GC002156.
Lu, Z., H. C. Jenkyns, and R. E. M. Rickaby (2010), Iodine to calcium ratios in marine carbonate as a paleo-redox proxy during oceanic anoxic events, *Geology*, *38*(12), 1107–1110, doi:10.1130/G31145.1.
Lu, Z., B. A. A. Hoogakker, C. Hillenbrand, X. Zhou, E. Thomas, K. M. Gutchess, W. Lu, L. Jones, and R. E. M. Rickaby (2016), Oxygen depletion recorded in upper waters of the glacial Southern Ocean, *Nat. Commun.*, *7*, 11146, doi:10.1038/ncomms11146.
Lu, Z. L., H. Tomaru, and U. Fehn (2011), Comparison of iodine dates from mud volcanoes and gas hydrate occurrences: Relevance for the movement of fluids and methane in active margins, *Am. J. Sci.*, *311*(7), 632–650, doi:10.2475/07.2011.03.
Lunt, D. J., P. J. Valdes, T. D. Jones, A. Ridgwell, A. M. Haywood, D. N. Schmidt, R. Marsh, and M. Maslin (2010), CO2-driven ocean circulation changes as an amplifier of Paleocene-Eocene Thermal Maximum hydrate destabilization, *Geology*, *38*(10), 875–878, doi:10.1130/G31184.1.

Lunt, D. J., et al. (2012), A model-data comparison for a multi-model ensemble of early Eocene atmosphere-ocean simulations: EoMIP, *Clim. Past*, *8*(5), 1717–1736, doi:10.5194/cp-8-1717-2012.

Ma, Z., E. Gray, E. Thomas, B. Murphy, J. Zachos, and A. Paytan (2014), Carbon sequestration during the Palaeocene–Eocene Thermal Maximum by an efficient biological pump, *Nat. Geosci.*, *7*, 382–388, doi:10.1038/NGEO2139.

Mangini, A., M. Jung, and S. Laukenmann (2001), What do we learn from peaks of uranium and of manganese in deep sea sediments? *Mar. Geol.*, *177*(1–2), 63, doi:10.1016/S0025-3227(01)00124-4.

McInerney, F. A., and S. L. Wing (2011), The Paleocene-Eocene Thermal Maximum: A perturbation of carbon cycle, climate, and biosphere with implications for the future, *Annu. Rev. Earth Planet. Sci.*, *39*, 489–516.

Nakayama, E., T. Kimoto, K. Isshiki, Y. Sohrin, and S. Okazaki (1989), Determination and distribution of iodide-iodine and total-iodine in the North Pacific Ocean - by using a new automated electrochemical method, *Mar. Chem.*, *27*(1–2), 105–116.

Neumann, T., U. Heiser, M. A. Leosson, and M. Kersten (2002), Early diagenetic processes during Mn-carbonate formation: Evidence from the isotopic composition of authigenic Ca-rhodochrosites of the Baltic Sea, *Geochim. Cosmochim. Acta*, *66*(5), 867–879, doi:10.1016/S0016-7037(01)00819-5.

Nicolo, M. J., G. R. Dickens, and C. J. Hollis (2010), South Pacific intermediate water oxygen depletion at the onset of the Paleocene-Eocene Thermal Maximum as depicted in New Zealand margin sections, *Paleoceanography*, *25*, PA4210, doi:10.1029/2009PA001904.

Norris, R. D., S. K. Turner, P. M. Hull, and A. Ridgwell (2013), Marine ecosystem responses to Cenozoic global change, *Science*, *341*(6145), 492–498, doi:10.1126/science.1240543.

Nunes, F., and R. D. Norris (2006), Abrupt reversal in ocean overturning during the Palaeocene/Eocene warm period, *Nature*, *439*(7072), 60–63, doi:10.1038/nature04386.

Olivarez Lyle, A., and M. W. Lyle (2006), Missing organic carbon in Eocene marine sediments: Is metabolism the biological feedback that maintains end-member climates? *Paleoceanography*, *21*, PA2007, doi:10.1029/2005PA001230.

Pälike, C., M. L. Delaney, and J. C. Zachos (2014), Deep-sea redox across the Paleocene-Eocene Thermal Maximum, *Geochem. Geophys. Geosyst.*, *15*, 1038–1053, doi:10.1002/2013GC005074.

Pierrehumbert, R. T. (2002), The hydrologic cycle in deep-time climate problems, *Nature*, *419*(6903), 191–198, doi:10.1038/nature01088.

Post, J. E., E. Thomas, and P. J. Heaney (2016), Jianshuiite in oceanic manganese nodules at the Paleocene-Eocene boundary, *Am. Mineral.*, *101*, 407–414.

Rathburn, A. E., and B. H. Corliss (1994), The ecology of living (stained) deep-sea benthic foraminifera from the Sulu Sea, *Paleoceanography*, *9*, 87–150, doi:10.1029/93PA02327.

Reid, P. C., et al. (2009), Impacts of the oceans on climate change, *Adv. Mar. Biol.*, *56*(9), 1–150, doi:10.1016/S0065-2881(09)56001-4.

Reitz, A., J. Thomson, G. J. De Lange, and C. Hensen (2006), Source and development of large manganese enrichments above eastern Mediterranean sapropel S1, *Paleoceanography*, *21*, PA3007, doi:10.1029/2005PA001169.

Ridgwell, A., and D. N. Schmidt (2010), Past constraints on the vulnerability of marine calcifiers to massive carbon dioxide release, *Nat. Geosci.*, *3*(3), 196–200, doi:10.1038/ngeo755.

Ridgwell, A., J. C. Hargreaves, N. R. Edwards, J. D. Annan, T. M. Lenton, R. Marsh, A. Yool, and A. Watson (2007), Marine geochemical data assimilation in an efficient Earth System Model of global biogeochemical cycling, *Biogeosciences*, *4*(1), 87–104, doi:10.5194/bg-4-87-2007.

Rosenthal, Y., E. A. Boyle, and N. Slowey (1997), Temperature control on the incorporation of magnesium, strontium, fluorine, and cadmium into benthic foraminiferal shells from Little Bahama Bank: Prospects for thermocline paleoceanography, *Geochim. Cosmochim. Acta*, *61*(17), 3633–3643, doi:10.1016/S0016-7037(97)00181-6.

Rue, E. L., G. J. Smith, G. A. Cutter, and K. W. Bruland (1997), The response of trace element redox couples to suboxic conditions in the water column, *Deep Sea Res., Part I*, *44*(1), 113–134.

Schenau, S. J., G. J. Reichart, and G. J. De Lange (2002), Oxygen minimum zone controlled Mn redistribution in Arabian Sea sediments during the late Quaternary, *Paleoceanography*, *17*(4), 1058, doi:10.1029/2000PA000621.

Scher, H. D., S. M. Bohaty, J. C. Zachos, and M. L. Delaney (2011), Two-stepping into the icehouse: East Antarctic weathering during progressive ice-sheet expansion at the Eocene-Oligocene transition, *Geology*, *39*(4), 383–386, doi:10.1130/G31726.1.

Shaw, T. J., J. M. Gieskes, and R. A. Jahnke (1990), Early diagenesis in differing depositional environments: The response of transition metals in pore water, *Geochim. Cosmochim. Acta*, *54*(5), 1233–1246, doi:10.1016/0016-7037(90)90149-F.

Sluijs, A., et al. (2006), Subtropical arctic ocean temperatures during the Palaeocene/Eocene Thermal Maximum, *Nature*, *441*(7093), 610–613, doi:10.1038/Nature04668.

Soliman, M. F., M. P. Aubry, B. Schmitz, and R. M. Sherrell (2011), Enhanced coastal paleoproductivity and nutrient supply in Upper Egypt during the Paleocene/Eocene Thermal Maximum (PETM): Mineralogical and geochemical evidence, *Palaeogeogr. Palaeoclimatol. Palaeoecol.*, *310*(3–4), 365–377, doi:10.1016/j.palaeo.2011.07.027.

Speijer, R. P. (1997), Benthic foraminiferal extinction and repopulation in response to latest Paleocene Tethyan anoxia, *Geology*, *25*(8), 683–686, doi:10.1130/0091-7613(1997)025<0683:BFEARI>2.3.CO;2.

Stassen, P., E. Thomas, and R. P. Speijer (2012), The progression of environmental changes during the onset of the Paleocene-Eocene Thermal Maximum (New Jersey Coastal Plain), *Austrian J. Earth Sci.*, *105*(1), 169–178.

Stassen, P., E. Thomas, and R. P. Speijer (2015), Paleocene-Eocene Thermal Maximum environmental change in the New Jersey Coastal Plain: Benthic foraminiferal biotic events, *Mar. Micropaleontol.*, *115*, 1–23, doi:10.1016/j.marmicro.2014.12.001.

Storey, M., R. A. Duncan, and C. C. Swisher (2007), Paleocene-Eocene Thermal Maximum and the opening of the northeast Atlantic, *Science*, *316*(5824), 587–589, doi:10.1126/science.1135274.

Stramma, L., G. C. Johnson, J. Sprintall, and V. Mohrholz (2008), Expanding oxygen-minimum zones in the tropical oceans, *Science*, *320*(5876), 655–658, doi:10.1126/science.1153847.

Tachikawa, K., C. Jeandel, A. Vangriesheim, and B. Dupré (1999), Distribution of rare earth elements and neodymium isotopes in suspended particles of the tropical Atlantic Ocean (EUMELI site), *Deep Sea Res., Part I*, *46*(5), 733–755, doi:10.1016/S0967-0637(98)00089-2.

Tebo, B. M., J. R. Bargar, B. G. Clement, G. J. Dick, K. J. Murray, D. Parker, R. Verity, and S. M. Webb (2004), Biogenic manganese oxides: Properties and mechanisms of formation, *Annu. Rev. Earth Planet. Sci.*, *32*(1), 287–328, doi:10.1146/annurev.earth.32.101802.120213.

Thomas, D. J., J. C. Zachos, T. J. Bralower, E. Thomas, and S. Bohaty (2002), Warming the fuel for the fire: Evidence for the thermal dissociation of methane hydrate during the Paleocene-Eocene Thermal Maximum, *Geology*, *30*, 1067–1070.

Thomas, E. (1989), Development of Cenozoic deep-sea benthic foraminiferal faunas in Antarctic waters, *Geol. Soc. London Spec. Publ.*, *47*, 283–296.

Thomas, E. (1990), Late Cretaceous through Neogene deep-sea benthic foraminifers (Maud Rise, Weddell Sea, Antarctica), in *Proceedings of the Ocean Drilling Program, Scientific Results*, vol. 113, edited by L. Mayer et al., pp. 571–594, Texas A & M Univ., College Station, Tex.

Thomas, E. (1998), Biogeography of the late Paleocene benthic foraminiferal extinction, in *Late Paleocene-Early Eocene Biotic and Climatic Events in the Marine and Terrestrial Records*, edited by M.-P. Aubry, S. G. Lucas, and W. A. Berggren, pp. 214–243, Columbia Univ. Press, New York.

Thomas, E. (2003), Extinction and food at the seafloor: A high-resolution benthic foraminiferal record across the Initial Eocene Thermal Maximum, Southern Ocean Site 690, *Geol. Soc. Am. Spec. Pap.*, *369*(303), 319–332, doi:10.1130/0-8137-2369-8.319.

Thomas, E. (2007), Cenozoic mass extinctions in the deep sea; what disturbs the largest habitat on Earth? in *Large Ecosystem Perturbations: Causes and Consequences*, *Spec. Pap*., vol. 424, edited by S. Monechi, R. Coccioni, and M. Rampino, pp. 1–24, Geol. Soc. of Am, Boulder, Colo.

Thomas, E., and N. J. Shackleton (1996), The Paleocene-Eocene benthic foraminiferal extinction and stable isotope anomalies, *Geol. Soc. London Spec. Publ.*, *101*, 401–441.

Tsunogai, S. (1971), Iodine in the deep water of the ocean, *Deep-Sea Research*, *18*, 913–919.

Waite, T. J., V. W. Truesdale, and J. Olafsson (2006), The distribution of dissolved inorganic iodine in the seas around Iceland, *Mar. Chem.*, *101*(1–2), 54–67, doi:10.1016/j.marchem.2006.01.003.

Weiss, R. F. (1970), The solubility of nitrogen, oxygen and argon in water and seawater, *Deep-Sea Res. Oceanogr. Abstr.*, *17*(4), 721–735, doi:10.1016/0011-7471(70)90037-9.

Wild, M., and B. Liepert (2010), The Earth radiation balance as driver of the global hydrological cycle, *Environ. Res. Lett.*, *5*(2), 25,203, doi:10.1088/1748-9326/5/2/025203.

Winguth, A., C. Shellito, C. Shields, and C. Winguth (2010), Climate response at the Paleocene-Eocene Thermal Maximum to greenhouse gas forcing—A model study with CCSM3, *J. Clim.*, *23*(10), 2562–2584, doi:10.1175/2009jcli3113.1.

Winguth, A. M. E., E. Thomas, and C. Winguth (2012), Global decline in ocean ventilation, oxygenation, and productivity during the Paleocene-Eocene Thermal Maximum: Implications for the benthic extinction, *Geology*, *40*(3), 263–266, doi:10.1130/g32529.1.

Wong, G. T. F., and P. G. Brewer (1977), Marine chemistry of iodine in Anoxic Basins, *Geochim. Cosmochim. Acta*, *41*(1), 151–159.

Zachos, J. C., D. Kroon, P. Blum, and E. Al (2004), Leg 208 summary, in *Proceedings of the Ocean Drilling Program*, vol. 208, pp. 2025–2030, Texas A & M Univ., College Station, Tex.

Zeebe, R. E., and J. C. Zachos (2007), Reversed deep-sea carbonate ion basin gradient during Paleocene-Eocene Thermal Maximum, *Paleoceanography*, *22*, PA3201, doi:10.1029/2006PA001395.

Zeebe, R. E., G. R. Dickens, A. Ridgwell, A. Sluijs, and E. Thomas (2014), Onset of carbon isotope excursion at the Paleocene-Eocene Thermal Maximum took millennia, not 13 years, *Proc. Natl. Acad. Sci. U.S.A.*, *111*(12), E1062–E1063, doi:10.1073/pnas.1321177111.

Zeebe, R. E., A. Ridgwell, and J. C. Zachos (2016), Anthropogenic carbon release rate unprecedented during the past 66 million years, *Nat. Geosci.*, *9*, 325–329, doi:10.1038/ngeo2681.

Zhou, X., E. Thomas, R. E. M. Rickaby, A. M. E. Winguth, and Z. Lu (2014), I/Ca evidence for upper ocean deoxygenation during the PETM, *Paleoceanography*, *29*, 964–975, doi:10.1002/2014PA002702.

Zhou, X., H. C. Jenkyns, J. D. Owens, C. K. Junium, X.-Y. Zheng, B. B. Sageman, D. S. Hardisty, T. W. Lyons, A. Ridgwell, and Z. Lu (2015), Upper ocean oxygenation dynamics from I/Ca ratios during the Cenomanian-Turonian OAE 2, *Paleoceanography*, *30*, 510–526, doi10.1002/2014PA002741.